Convention Special Issue – 2020

J. Indian Chem. Soc.,
Vol. 97, No. 12a, December 2020, pp. 2699-2712

A comparative analysis of Ru(II) complexes containing non-annulated and annulated N-heterocyclic carbene ligand towards structure, spectra, electrochemistry and biological activity†

Bidyut Kumar Rana*[a,b], Joydev Dinda*[c], Himadri Sekhar Das[a], Marlon Hemrique Cardoso[d,e], Octávio Luiz Franco[d,e], Partha Pratim Bag[f], Pradip Kumar Mahapatra[b], Santanab Giri[a] and Gourisankar Roymahapatra*[a]

[a]School of Applied Science, Haldia Institute of Technology, Haldia-721 657, West Bengal, India

[b]Department of Chemistry, Jadavpur University, Kolkata-700 032, India

[c]Department of Chemistry, Utkal University, Bhubaneswar-751 004, Odisha, India

[d]S-Inova Biotech, Programa de Pós-Graduação em Biotecnologia, Universidade Católica Dom Bosco, Campo Grande, Brazil

[e]Centro de Análises Proteômicas e Bioquímicas, Programa de Pós-Graduação em Ciências Genômicas e Biotecnologia, Universidade Católica de Brasília, Brasília, Brazil

[f]Department of Chemistry, School of Basic Science, SRM University Sikkim, Gangtok-737 102, Sikkim, India

E-mail: gourisankar1978@gmail.com, rana_bidyut@yahoo.com, joydevdinda@gmail.com

Manuscript received online 02 December 2020, revised and accepted 27 December 2020

A new Ru-N-heterocyclic carbene (Ru-NHC) complex (**3a**), chloro(*p*-cymene)-1-methyl-3-pyrimidylimidazolideneruthenium(II)-hexafluorophosphate was synthesized from a non-annulated NHC precursor,1-methyl-3-pyrimidylimidazolium-hexafluorophosphate (**3**). The half-sandwich geometry of the molecule is established with single crystals X-ray diffraction. The absorption spectra and electrochemical nature of the complex are also investigated, supported by DFT analysis. Compound **3a** is applied on lung (A549), colon (HCT116), and breast (MCF7) cancer cells to examine their *in vitro* cytotoxicity activity, and results are summarized and compared with a recent report for Ru(II)-NHC complexes containing annulated NHC ligands.

Keywords: Ru(II)-NHC, half-sandwich geometry, spectra, electrochemistry, DFT, cytotoxicity, molecular docking.

Introduction

The discovery of *cis*platin in 1969 by Rosenberg[1] shaped the future research attention to developing new metal-based antitumor drugs. For Pt-based anticancer drugs, genomic DNAs are the main cellular targets. Exclusively for *cis*platin, it has been observed that the main antitumor activity instigates intra-strand cross-linking and DNA kinking[2]. Therefore, DNA targeting molecules remain in the public interest. Therefore, the target-specific molecules acting selectively towards cancer cells over normal cells attain more contemplation[3]. The remarkable success of *cis*platin over cancer cells impelled the possibility of synthesizing alternative metal-based anticancer drugs, with the possibility to overcome different types of carcinoma[4]. Although *cis*platin has long been used as an antitumor drug, it suffers from dose-limiting nephrotoxicity and drug resistance potential efficacy[5]. As a less toxic alternative, ruthenium complexes propose excellent architect alternative anticancer compounds[6]. Interest in ruthenium-

†**Authors B. Rana, J. Dinda, S. Giri and G. Roymahapatra, want to dedicate this article to treasure the beautiful times with Professor Chittaranjan Sinha (popularly known as CRS sir), on his upcoming 61st birthday (DOB: 2nd April 1961). CRS sir will always be in our heart for his simplicity and unique teaching style.**

based complexes arises from the synthesis of ruthenium(III) ammine complex, $RuCl_3(NH_3)_3$ by Clarke *et al.*[7]. They reported that Ru-based complexes are more soluble and exhibit higher efficacy as anticancer and antitumor agents[8,9]. The chemical resemblance of the platinum (Pt) group metals (Pd, Rh, Ir, Ru, and Os) complexes is also a matter of great interest for antitumor therapies[10]. After the stable isolation of bottleneck N-heterocyclic carbene (NHC)[11], which comprises a flexible and indispensable group of ligands for a broad array of transition metals[12], NHC-metal complexes are found to be a new class of alternative lead anticancer drug candidates. NHCs, familiar as 'phosphine mimics' in chemical science, can bind with transition metals with a strong bond and form highly stable complexes against air, moisture, and heat[11–15]. They have versatile applications starting from catalysis, biomedical, electrochemical, luminescent, among other activities[12–15].

Ag(I)-NHC complexes are easier to synthesize in the M-NHC category (M = Metal), and they have attracted attention due to their therapeutic efficiency[16,17], specifically for cancer treatments and also as an alternative to combat drug-resistant pathogens[18,19].

In the coinage metal group, Au(I) analogs also hold excellent potential[20]. Indian alchemy documented gold (Au) as medicine from the pre-Vedic period and found it active against cancer[21–23]. It has been demonstrated that, due to its non-toxic nature and better solubility, a series of ruthenium complexes are taken into clinical trials for anticancer and antitumor therapies[24–28]. The report on the anticancer activity of [Ru(II)-(η^6-arene)-(en)Cl][PF_6] compound in both *in vitro* and *in vivo*[29], including efficacy against *cis*platin-resistant cancer cells, makes Ru-NHC complexes more tempting as scaffolds for drug design, due to their slow ligand dissociation rate in biological systems[30]. Ru-arene complexes are distinctly inactive in normal cells of biological systems[31,32] and have also been used in anticancer treatments. By contrast, due to the concentration gradient between inter/extra-cellular chloride concentrations, ruthenium-chloro complexes show better transportation towards object cells[33]. The drug activation occurs when chloride dissociates from one ruthenium coordination site and makes that metal site exposed and capable of binding to cancer cells' DNA[33]. Inspired by current findings, we have recently reported two ruthenium complexes, named **1a** and **2a**; [Ru(II)-(*p*-cymene)-(L)Cl][PF_6], (L = corresponding NHC ligand) (Fig. 1), and studied their

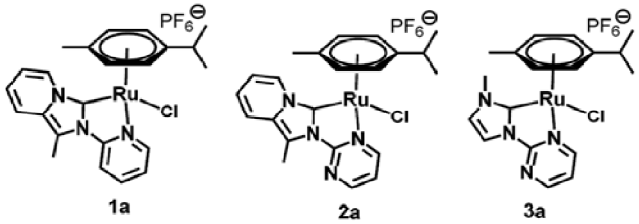

Fig. 1. Schematic diagram for the complexes **1a**, **2a**, and **3a**.

structures, electronic spectra, electrochemistry, cytotoxicity, and binding properties trough molecular docking simulations[34]. Here, we report a new pyrimidine (Pym) functionalized non-annulated half-sandwich Ru(II)-NHC complex, denominated **3a**, and compared our main findings with those recently reported[34] for compounds **1a** and **2a**.

Results and discussion

Synthesis and elementary analysis:

The non-annulated imidazolium proligand, 1-methyl-3-pyrimidylimidazolium-hexafluorophosphate **(3)** was prepared as previously reported[35] using the neat reaction of 1-methylimidazole and 2-chloropyrimidine with stoichiometric amounts in a pressure-sealed tube at 90–95°C, refluxing in toluene bath for 6 h, without using solvent, followed by anion metathesis by saturated KPF_6 solution. The imidazolium salt (proligand) was recovered with a good yield. Elemental analyses, including ^{1}H NMR, ^{13}C NMR, and absorption spectroscopy, were used to characterize the proligand (**3**). In DMSO-d_6 solvent, the ^{1}H NMR spectra of compound **3** show a downfield resonance at δ 9.86 ppm, which is a characteristic of the NC*H*N imidazolium proton[33–35].

The complex **3a**, [Ru(η^6-*p*-cymene)(3-H)Cl][PF_6] was prepared *in situ* using the transmetallation protocol from an Ag-carbene[34,35] complex of the proligand **(3)**. The reaction of [Ru_2(*p*-cymene)$_2Cl_4$] with the Ag-NHC complex in ACN solvent at room temperature resulted in the complex **3a** (Scheme 1) as air-stable yellowish-orange solids. The development of complex **3a** was distinctly identified from the absence of NC*H*N imidazolium proton (in ligand **3**) at 9.86 ppm in its ^{1}H NMR spectra.The position and integrated intensity of other protons of the imidazolium fragment range from δ 8.73–7.85 ppm. In the ^{13}C NMR spectrum of **3a**, the carbenic carbon N***C***HN and α-carbon of pyrimidine shift from 24.0 to 14.8 ppm more than free ligand **3**.

The complex **3a** is soluble in general organic solvents,

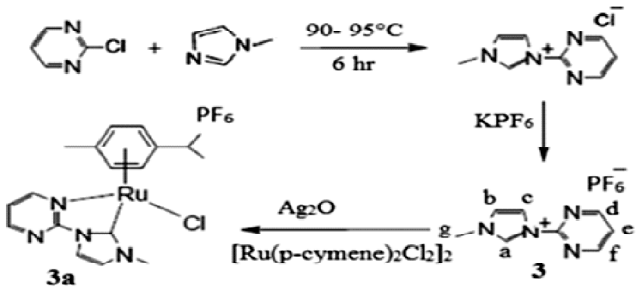

Scheme 1. Synthetic protocol for ligand **3** and complex **3a**.

including DMF and DMSO, and poorly soluble in water. The compound was fully characterized by elemental analysis and spectroscopy. The solid-state structure was analyzed by the single-crystal X-ray diffraction (XRD) technique.

Crystal structure:

The single-crystal XRD structure reveals that **3a** presents a pseudo-octahedral and half-sandwich geometry[34,36,37]. The molecular structure of **3a** is shown in Fig. 2. Complex **3a** crystallizes in the monoclinic crystal system (space group: $P2_1/n$). The Ru center is bonded with pyrimidine nitrogen N(4), carbene C(1), Cl(1) of ligand **3**, and *p*-cymene ring in an η^6 manner[34] (considering the *p*-cymene rings as a single coordinating site) to satisfy the coordination of pseudo-octahedral geometry. The crystallographic parameters are listed in Table 1, and bond parameters are listed in Table 2. The crystallographic unit of **3a** has two asymmetric units, and counter anion PF_6 is present.

The *p*-cymene ring in the present complex is almost planar[34], and the Ru(II) center is at a distance of 1.716(4) Å

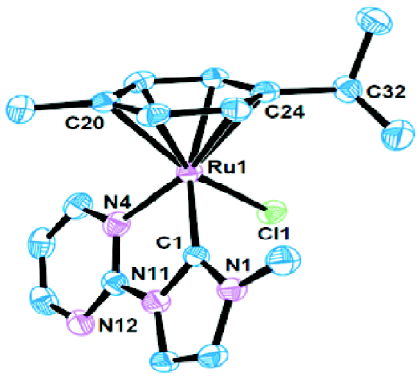

Fig. 2. ORTEP view (40% probability) of single-crystal X-ray structure of **3a** (hydrogen and PF_6 have been removed for clarity).

Table 1. X-Ray experimental data for the complex **3a**

Parameters	**3a**
Formula	$[C_{18}H_{22}ClN_4Ru]^+,PF_6^-$
MW	575.89
Temp. (K)	293(2)
Crystal system	monoclinic
Space group	$P2_1/n$
a (Å)	14.1263(11)
b (Å)	18.4047(15)
c (Å)	16.7018(13)
β (°)	98.939(2)
Volume (Å^3)	4289.6(6)
Z	8
θ - range	1.66–28.99
Index ranges	$-18 \le h \le 19$; $-22 \le k \le 23$; $-22 \le l \le 21$
Absorp. coeff. (mm^{-1})	0.995
No. of reflns. collected	10653
No. of ind. reflns.	7172 [R(int) = 0.0556]
Goodness of fit (GOF)	1.090
Final *R* indices	R1 = 0.0490,
[I > 2σ (I)]	wR2 = 0.1363
R indices (all data)	R1 = 0.0870, wR2 = 0.1680
Largest diff. peak and hole (e Å^{-3})	1.79 and –1.32
CCDC number	824311

Table 2. Selected bond lengths (Å) and angles (°) for the complex **3a**

	3a
Ru(1)-C(1)	2.017(4)
Ru(1)-N(3)	2.099(4)
Ru(1)-Cl(1)	2.4036(1)
Ru(1)-C_{cent}	1.716(4)
C(1)-N(1)	1.389(5)
C(1)-N(2)	1.336(5)
C(1)-Ru(1)-Cl(1)	85.23(12)
C(1)-Ru(1)-N(3)	77.00(16)
N(1)-C(1)-N(2)	103.3(3)
C_{cent}-Ru(1)-Cl(1)	126.32

from the centroid of the arene ring (*p*-cyemen). The Ru-Cl bond distance is 2.4036(11) Å is standard and comparable with our recent report[34], as well as other findings[38]. The C(L)-Ru-Cl bond angle is found to be 85.23(12)° in complex **3a** and comparable to our recent report [86.57° (**1a**) and 86.33° (**2a**)]. The N-C bond distances of imidazolidine {C(1)-N(1) = 1.389(5) Å and C(1)-N(2) = 1.336(5) Å} in the asymmetric

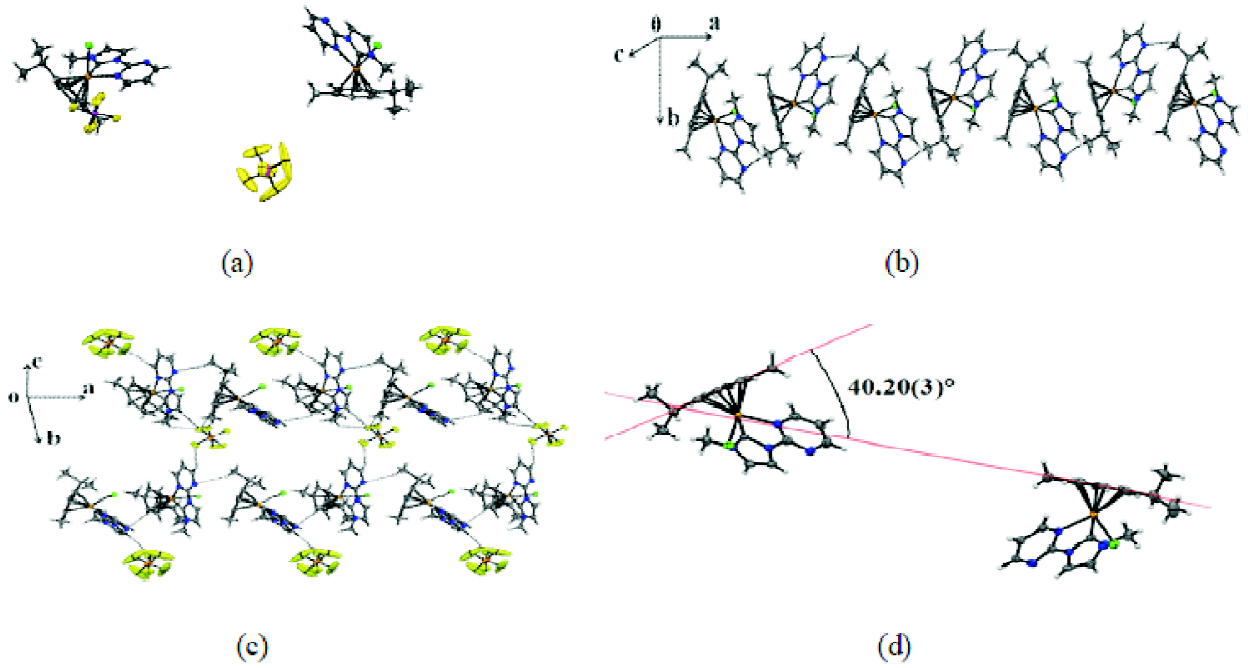

Fig. 3. (a) Asymmetric unit of **3a**; (b) packing of 1D chain structure propagating along *a*-axis; (c) packing of 2D chain structure along *ab* plane and (d) angle between two phenyl rings of *p*-cymene of two entities.

unit are different, which are slightly shorter than a single C-N bond (1.47 Å) and indicating the presence of double bond character. The internal bond angle N(1)-C(1)-N(2) = 103.3(3)° is comparable with our recent report[34] and also with the other imidazolidine systems[42].

The asymmetric unit of the complex with PF_6 as counter anion is shown in Fig. 3a. It forms a 1D chain structure propagating along *a*n a-axis (Fig. 3b). Moreover, it forms a 2D chain where PF_6 anion acts as a bridge along *the ab* plane (Fig. 3c). In the pseudo-octahedral geometry of the complex, the arene ring occupies one face of the octahedron. The coordination style of Ru(II) center with chloride ion and one pyrimidine nitrogen 'N(1)' and $C_{carbene}$ 'C(1)' of ligand **3** and Ru(II)-π interactions with *p*-cymene in η^6 manner is shown in Fig. 3a. The Ru-N_{pym}, Ru-$C_{carbene}$, and Ru-Cl bond distances in the complex **3a** are 2.099(4) Å, 2.017(4) Å, and 2.4036(1) Å in that order, and the values are in agreement with previously reported complexes[34,38–41]. Two phenyl ring of *p*-cymene of two entities (Fig. 3d) makes an angle 40.20(3)°. The crystal packing (Fig. 3c) is stabilized by a combination of C-H···N, C-H···F, C-H···Cl, C-H···π, and anion···π interactions.

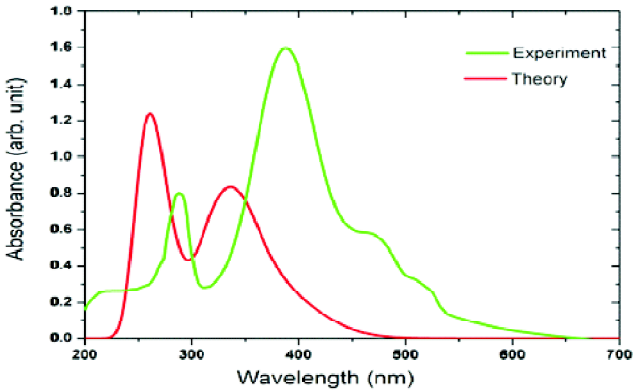

Fig. 4. Absorption spectra of complex **3a** in ACN solvent at room temperature; experimental (green) and theoretical (red).

Electronic spectra:

Absorption spectra of Ru(II)-NHC complex **3a** in ACN solvent are shown in Fig. 4, and significant transition values of absorption spectra are listed in Table 3. The moderately intense band at 288 nm is owing to ligand-oriented transitions. However, the absorption bands near 385 nm could have substantial metal donations in the complex. The absorption maxima (385 nm) for **3a** is found in between reported com-

Table 3. Primary transition values in absorption spectra of complex **3a** (experimental and theoretical data)

Wavelength (nm)		Osc.	Major transitions
Expt.	Theory	strength	
288	262	0.0443	H-4- > LUMO (71%), H-4- > L+1 (12%)
	263	0.0324	H-1- > L+5 (68%), H-1- > L+3 (4%), H-1- > L+4 (5%)
385	336	0.0301	H-2- > LUMO (76%), HOMO- > L+3 (11%), H-2- > L+2 (3%), HOMO- > L+5 (2%)
	338	0.0301	H-2- > L+1 (10%), H-1- > LUMO (15%), H-1- > L+1 (13%), HOMO- > L+1 (18%), HOMO- > L+2 (27%)

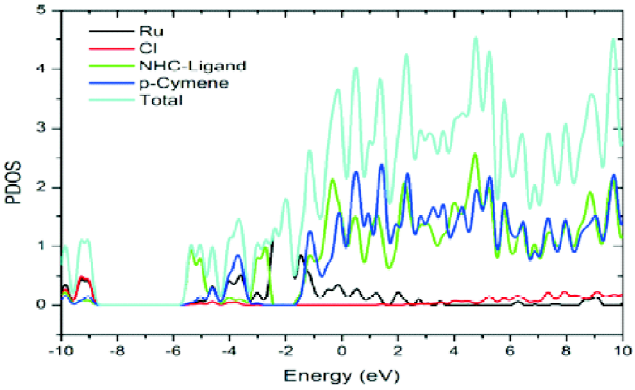

Fig. 5. Partial density of states (PDOS) for complex **3a**.

plex **1a** (372 nm) and **2a** (403 nm)[34]. The absorption maxima of **3a** are ~13 nm red-shifted from complex **1a**, because of electron-rich pyrimidine ligand and ~18 nm blue-shifted from **2a** of a non-annulated 1-methyl imidazole fragment. A distinct blue shiftis found compared to $[Ru(bpy)_3]^{2+}$, due to solid σ-donor and weak π-acceptor character of pyrimidine functionalized NHC ligand compared to bi-dentate bipyridine ligand[43a]. The MLCT type transitions in absorption spectra are supported by computational calculations[43b] in the DFT platform (Fig. 4, Table 3) by implementing B3LYP/def2-TZVP basis set[34] with Gaussian 09 W software.

The theoretical λ_{max} values 25~50 nm varied from experimental values. The calculated transitions at 262–263 nm (288 nm in expt.) involve a significant contribution from HOMO-1→LUMO+5 (68%), HOMO-4→LUMO (71%), HOMO-4→LUMO+1 (12%). Transitions at 336–338 nm (385 nm in expt.) involve HOMO-2→LUMO (76%), HOMO-→LUMO+2 (27%), HOMO→LUMO+1 (18%), HOMO-1→LUMO (15%) (Table 3). To get insight into the structure bonding correlation on the electronic transition of absorption spectra, we have analyzed PDOS[34,44] using computational techniques. The metal and ligand contributions to the formation of FMOs (Fig. 5) were also calculated in the same level of theory; B3LYP/def2-TZVP. The compositions of occupied FMOs show that these have significant Ru contribution (30 ~ 40%), except for HOMO-5 (Ru, 14%), and some of the occupied MOs also contain a high contribution from coordinated Cl (36~45%). The unoccupied MOs exhibit a major share from NHC ligand (LUMO, 93%; LUMO+1, 76%), and *p*-cymene contributes to the LUMO of higher energy level (LUMO+3~LUMO+5, 44~65%) (Fig. 5, Table 4). Hence, in-

Table 4. Orbital contribution (%) towards the formation of frontier molecular orbitals (FMOs)

FMOs	Orbital energy (eV)	Contribution of Ru (%)	Contribution of Cl (%)	Contribution of ligand-**3** (%)	Contribution of *p*-cymene (%)
LUMO+5	–3.54	43	0	8	49
LUMO+4	–3.75	26	4	5	65
LUMO+3	–4.02	39	4	13	44
LUMO+2	–4.60	33	6	31	30
LUMO+1	–5.03	7	3	76	14
LUMO	–5.37	2	1	93	4
HOMO	–9.02	38	40	7	14
HOMO-1	–9.31	41	45	7	6
HOMO-2	–9.85	36	27	21	16
HOMO-3	–10.23	30	22	43	5
HOMO-4	–10.54	41	36	17	6
HOMO–5	–11.10	14	18	51	16

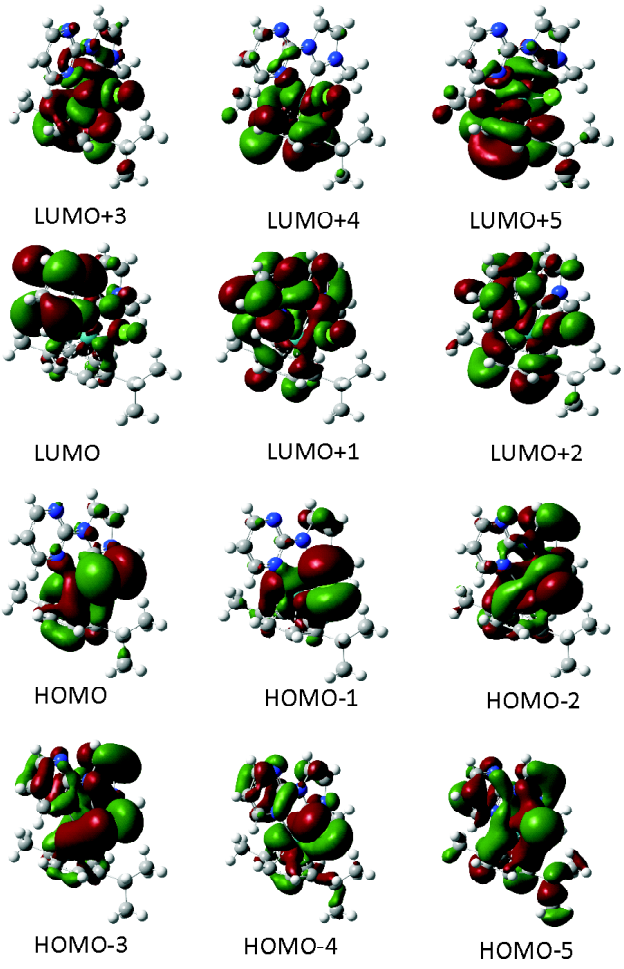

Fig. 6. Frontier molecular orbitals (FMOs) for complex **3a**.

stead of pure ligand characteristics (intra-ligand/inter-ligand) transitions, the complex **3a** bears a mixed-mode of metal-ligand transitions. Under oxygen-free conditions, complex **3a** isfound to be nonemissive in ACN at room temperature. Some selective FMOs are shown in Fig. 6.

Electrochemistry:

The electrochemical nature of complex **3a** was analyzed by cyclic voltammetry (CV) at a stationary Pt-electrode in deoxygenated ACN solvent (*ca*. 5×10^{-4} *M*) at 25°C.The reference electrode Ag/AgCl was used with 0.1 *M* TBAH as the supporting electrolyte in +2.5 to –1.5 eV range. In cyclic voltammograms (Fig. 7) for complex **3a**, two consecutive irreversible oxidation peaks were found. The computational study replicates the complex character of the redox process. In comparison to our recent report[34], here we also observed

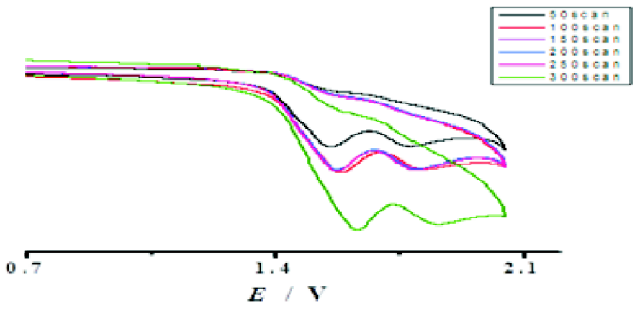

Fig. 7. Cyclic voltammograms of **3a** were recorded in dry ACN. Conditions: scan rate = 200 mV s^{-1} and using a cell that was equipped with a Pt working electrode, an Ag/AgCl reference electrode, and $[N(Bu)_4](PF_6)$ (0.1 *M*) as supporting electrolyte.

that no reduced peak appears subsequently to two oxidized signals at 1.62 V, 1.84 V. Composition of FMOs (Table 4) supports this data. Oxidation means take out electrons from the occupied MO, and the opposite occurs for reduction processes. From Table 4, we observed that the oxidation is not related to the metal character only; rather, the HOMO and other filled MOs consist of Ru, Cl, and NHC. When oxidized species immediately allocate charge over the composed partners, the character of the species on the electrode surface is lost and, therefore, the reduction of the identical species is not established. The electron population at unoccupied MOs refers to the cathodic response. In this case, the same tendency is noticeable (that is, no explicit function is recognizable), and CV does not show any distinct reduction wave, and thus experiment substantiates with the DFT results. The result is congruent with our recent report[34] and other Ru(II)-NHC complexes[45]. According to Ang *et al.*[46] the redox signal of the Ru(η^6-arene) unit is greatly governed by the arene ligand and its number of alkyl substituents[46]. The bulky size of *p*-cymene ring certainly persuades the irreversibility of Ru(II)/Ru(III) redox path and retards the absorption of the complex compound on the electrode surface. On the variation of scan rate, the E_{pa} value shows insignificant change (<10%), which implies a steady redox state with electron removal from the HOMO during the electrochemical process. Thus, the chemical structure is stable under the influence of electrode potential.

Cytotoxic activity:

The Ru-complex **3a** was evaluated for its cytotoxic properties. This complex is soluble in organic solvents DMSO/

DMF, but not in water. We have studied the *in vitro* cytotoxic effects of complex **3a** on lung (A549), colon (HCT116), and breast (MCF7) cancer cell lines as previously described[34,47,48], at varying molar concentrations. The compound was also studied on non-carcinoma 3T3 cells (embryonic fibroblast of a healthy mouse). The results are summarized in Table 5. For A549, the half-maximal inhibitory concentration (IC_{50}) value for **3a** is 9-fold lower than **1a** and slightly higher than **2a**. For HCT116 cells, the IC_{50} for **3a** is nearly 50-times lower than **1a** and 11-times lower than **2a**. When evaluated on MCF7 cells, the complex **3a** presents an IC_{50} 3-fold lower than **1a** and 1.5-fold higher than **2a**[34]. Finally, the complex **3a** was highly efficient against all cancer cell lines tested[49,50] compared to *cis*platin.

Table 5. IC_{50} values (μM) against A549, HCT116, MCF7 cell lines

Complex	**3a**	**1a** [Ref. 34]	**2a** [Ref. 34]	*Cis*platin
A549	2.8±0.4	28.7±2.3	2.1±0.7	64
HCT116	2.3±0.3	>100	8.6±1.8	23.2
MCF7	4.7±0.7	14.8±2.3	3.3±0.4	13
3T3	8.56±1.6	44.64±2.6	9.36±1.16	64

We have studied the cell viability (change of optical density) of all three compounds, including **1a**, **2a**, **3a**, on three different cell lines of different origin and compared these results in Fig. 8 to evaluate the antineoplastic activity of these compounds. We have observed that compounds **3a** and **2a** present 3 to 4-times better antineoplastic activity than **1a**[34] and *cis*platin (Fig. 8).

We have also studied the DNA cleavage activity of complex **3a** (Fig. 9). Two types of DNA scission are observed in these systems, leading to a nicked/relaxed plasmid (form II) and a linear DNA (form III). These two products may be separated effectively from the substrate, the supercoiled plasmid (form I). We have used **3a** at 500 nM, given that at 250 nM to 1 μM, the same plasmid DNA form II is generated. It is observed that cleavage starts after 1 h reaction. Almost 10% of DNA form II is produced after a reaction time of 3 h, which remains almost unchanged up to 9 h (Fig. 9). Remarkably, form II is found to be double in percentage after 10 h incubation. These features reflect the ability of ruthenium to perform direct double-strand breaking. The DNA conformational changes induced by Ru-complex **3a** were investigated by circular dichroism (CD) spectroscopy. The samples containing CT-DNA in a concentration of 50 μg mL^{-1} in the presence or absence of compound **3a** (250 nM and 500 nM) in

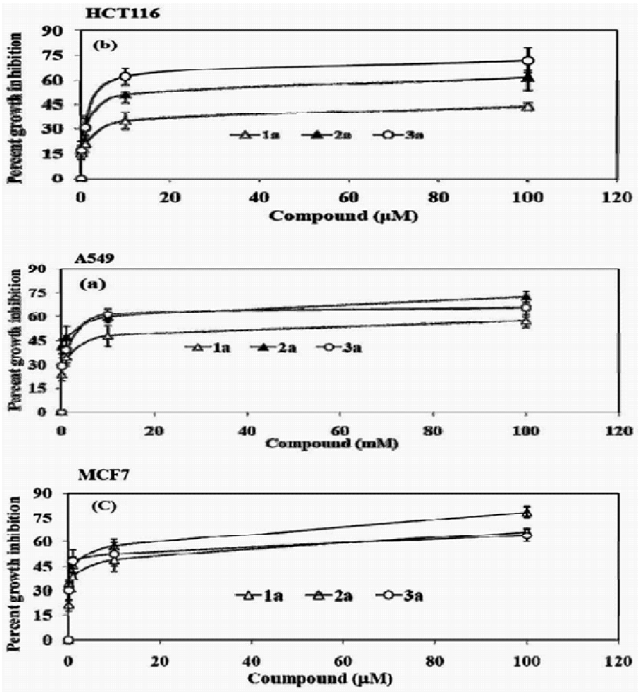

Fig. 8. Cell viability assay. 2×10^5 cells were treated with varying concentrations [0–100 μM] of complexes **1a**, **2a** [Ref. 34], and **3a** for 24 h, and an MTT assay was performed. O.D. at 595 nm presents the viability of (a) A549 (b) HCT116 and (c) MCF7 cells. Results are from one of the three representative experiments. Values are mean - S.D.

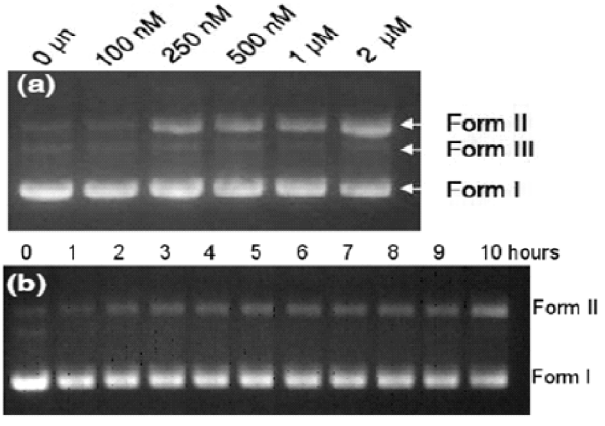

Fig. 9. (a) Gel mobility shift assay of circular pTZ57R/T plasmid DNA by complex **3a**; (b) time-dependent gel mobility shift assay pTZ57R/T plasmid DNA by complex **3a**.

10 mM phosphate buffer (pH 7.2) were recorded. The ionic strength was kept constant, and the R-value remained constant at 0.1. CD spectra were recorded at 37°C. The changes observed in the native right-handed B-form DNA upon interaction with the compound are shown in Fig. 10.

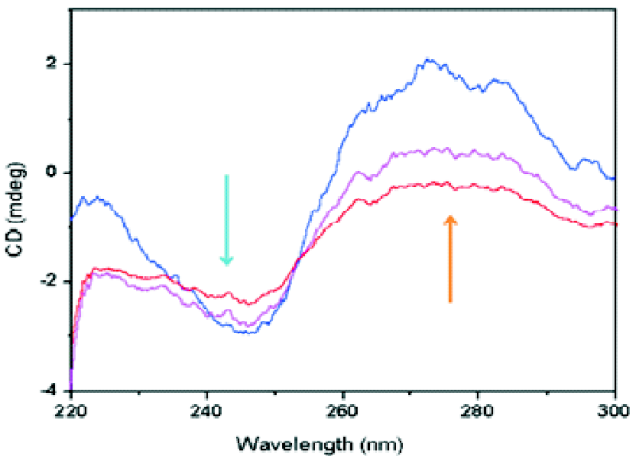

Fig. 10. Circular dichroism (CD) spectra of native right-handed B-form DNA (blue line) 250 nM, Ru(II)-complex (**3a**) at 250 nM (magenta line) and 500 nM (red line).

The right-handed B-DNA exhibits remarkable transformations in its positive and negative bands at 272–275 nm and 248–250 nm, respectively, upon interaction with complex **3a** (Fig. 10). Complex **3a** induces a decrease in intensity for both the positive (272 nm) and negative bands (248 nm). A new, negative band observed at 230 nm indicated the degradation of DNA structure. The diminished intensity in the positive band indicates destabilization of base-stacking, and the decrease in the negative band intensity specifies a loss in right-handed helicity[51]. The orderly diminution in the intensities of the bands revealed a consistent, explicit type of interaction of complex **3a** with DNA. The observed changes in the total loss of DNA helicity or DNA unwinding suggest the strong interaction of **3a** with DNA. Dyson and Sadler first explored the anticancer activity of Ru-arene complexes[52].

Moreover, the fundamental blueprint of this type of compound and its mechanisms of action were reviewed previously[53]. In this perspective, it should be reminiscent that Ru(II) compounds display low toxicity in response to other metals. Although detailed research is required to unravel their mechanism of action, it is supposed that Ru-compounds are exclusively gathered in fast-breaking cells, such as a tumor. It happens due to the capacity of Ru to mimic Fe (iron) in binding to transferrin[54] with proteins that supply iron to cells, and transferrin receptors are over uttered in cancer cells[55]. Secondly, *in vivo* studies have shown that Ru(II)-compounds present high kinetic and thermodynamic stability and, therefore, may be recommended as antitumor drugs[56a]. In this context, it should also be noted that Ru(II)-compounds exhibit promising thermodynamic and kinetic stability and low toxicity in comparison to other metals[56,57]. Complex **3a** is efficient compared to other reported Ru(II)-arene complexes with anticancer properties[34].

Molecular docking studies:

The molecular docking analysis is a suitable tool to investigate the interactions between proteins and bioactive molecules (e.g. metallodrugs) in theiratomic levels[58]. It lends a hand to exemplify the nature of the bioactive molecule towards the binding site of target proteins and shed light on the elemental biochemical progression. Our experimental findings included cytotoxic assays, DNA binding, and CD spectroscopy with complex **3a**, molecular docking (Fig. 11) studies were performed. The crystal structure of a B cell CLL/lymphoma 2 (BCL-2) (PDB entry: 4lvt)[59] protein member and a DNA dodecamer (PDB entry: 1bna)[60] were used as primary targets. BCL-2 is a member of the BCL protein family and was selected for molecular docking studies because it is a key regulator of apoptosis by controlling the outer membrane permeabilization of mitochondria[61]. Apart from this, complex **3a** binding affinity was also predicted in contact with a DNA strand (Fig. 11). The predicted binding affinities are summarized in Table 6.

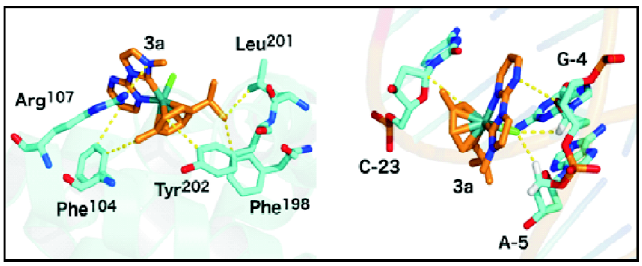

Fig. 11. Complex **3a** docked with BCL-2 (left) and DNA (right), respectively. BCL-2 residues and DNA nitrogenous bases involved in atomic interactions are highlighted as cyan sticks.

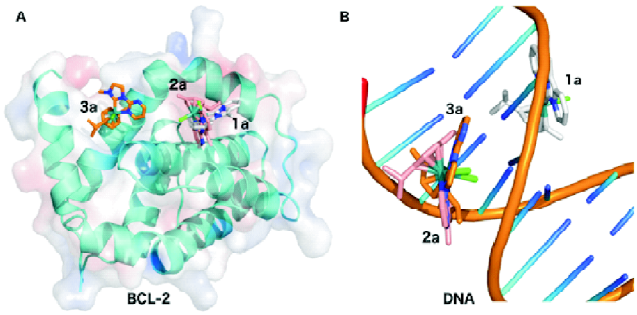

Fig. 12. Superpositionof complexes**1a**, **2a** [Ref. 34] and **3a** bound to BCL-2 (A) and DNA (B). **1a** is represented as white sticks, **2a** as light pink sticks, and **3a** as orange sticks. Adaptive Poisson-Boltzmann solver (APBS) electrostatic potential of BCL-2 (A), with potentials ranging from – 5 kT.e^{-1} (red) to + 5 kT.e^{-1} (blue).

Table 6. Predicted binding affinities (kcal mol^{-1}) for the molecular complex heterocyclic carbenes-DNA and BCL-2

Complex	**3a**	**1a** [Ref. 34]	**2a** [Ref. 34]
BCL-2	–7.1	–6.7	–7.0
DNA	–7.3	–7.3	–8.2

Compared with our previous computational data reported for complexes **1a** and **2a**, we observed that complex **3a** binds to a different hydrophobic pocket in BLC-2 with the highest binding affinity, whereas both complexes **1a** and **2a**[34] bind to the same region. Interestingly, the opposite is observed when these complexes are simulated in contact with a DNA strand, as the complexes **3a** and **2a**[34] are superimposed, whereas complex **1a** binds to the other side of the DNA strand. Nevertheless, although complex **3a** and **2a**[34] bind to the same position in the DNA, the binding affinity predicted for **2a**[34] is higher than **3a**. Finally, according to the results summarized in Tables 7 and 8, the **3a**-BCL-2 molecular complex is stabilized mainly by hydrophobic interactions and a single hydrogen bond. By contrast, hydrogen bonds, H-boding (H···Cl), and hydrophobic interactions were predicted for the complex **3a**-DNA. Similar patterns of atomic interactions were predicted in our recent study for complex **1a** and **2a** in contact with BCL-2 and DNA[34].

Table 7. Predicted atomic interactions between BCL-2 and complex **3a**

BCL-2 (PDB entry: 4lvt)			Complex **3a**		
Residue	Position	Atom name	Distance (Å)	Atom name	Compound
Phe	104	CD1	3.6	C36	**3a**
Phe	104	CE1	3.4	C35	**3a**
Arg	107	NH1	3.5	N5	**3a**
Phe	198	CE1	3.4	C35	**3a**
Leu	201	CD2	3.5	C35	**3a**
Tyr	202	CE1	3.6	C29	**3a**

Table 8. Predicted atomic interactions between DNA and complex **3a**

DNA (PDB entry: 1bna)			Complex **3a**		
Residue	Position	Atom name	Distance (Å)	Atom name	Compound
Cytosine	23	C1	3.5	C31	**3a**
Adenine	5	C5	2.9	H···Cl	**3a**
Guanine	4	C1	2.8	H···Cl	**3a**
Guanine	4	O4	3.6	N8	**3a**

Experimental

Materials:

The synthesis of proligand **3** and the corresponding Ru complex **3a** was prepared under an open atmosphere otherwise stated. All the required reagents 1-etylimidazole, 2-chloropyrimidine, Ag_2O, KPF_6 and [Ru(*p*-cymene)Cl_2]$_2$ used in this synthesis were purchased from Sigma Aldrich and used without further purification. All solvents (ACN, THF, and DMSO) were distilled over suitable drying agents. NMR spectra were recorded at room temperature using DMSO-d_6 as a solvent on a Bruker 300 Mz NMR-spectrometer with TMS as internal standard. Elemental analyses were performed using a Perkin-Elmer 2400C analyzer. The absorption spectrum of the complex was recorded with a Shimadzu UV-1601. Electrochemical data were collected with a PAR model 273A, and EI-mass spectra were recorded on an Esquire 3000 plus instrument.

*Synthesis of 1-methyl-3-pyrimidylimidazolium-hexafluorophosphate (**3**):*

The proligand **3** was synthesized by mixing *N*-methylimidazole and 2-chloropyrimidine as previously reported[35]. *N*-methylimidazole 2.0 g (24.7 mmol) and 2-chloropyrimidine 3.0 g (26.5 mmol) were stirred in a sealed tube using neat reaction (without solvent) condition at the 90–95°C in an oil bath for 6 h, which lead to the formation of light brown solid with significantly good yields. The resulting crude solid was

washed with dry THF and shaken in a mechanical shaker for 1 h to eliminate impurities, and the process was repeated 2-3 times to get the pure product of 1-methyl-3-pyrimidylimidazolium chloride, and the product was then dried in a vacuum. Dried solid chloride salt was converted to its PF_6 salt using the simple anion transferred method; by dissolving the chloride salt in a minimum amount of distilled water and then added with excess saturated aqueous KPF_6 solution. White ppt of compound **3** was formed immediately. The ppt was filtered, washed with ether, dissolved in ACN solvent, recrystallized from ACN and diethyl ether. The solid mass was dried in a vacuum. The product formed with satisfactory yield with 72% (2.56 g, 7.18 mmol). ^{1}H NMR (DMSO-d_6, 25°C, 300 Mz, ppm) δ: 9.86 (s, 1H^a, NC*H*N), 8.72 (d, 2H^{d,f} *J* 3.8 Hz), 8.36 (s, 1H^c), 7.94 (s, 1H^b), 7.68 (t, 1H^e *J* 4.5 Hz), 3.61 (s, 3H^g, CH_3). ^{13}C NMR (DMSO-d_6, 25°C, 400 Mz, ppm) δ: 157.8 (*m*-C of pym.), 149.6 (NCN of pym.), 134.8 (NC*H*N), 124.2 (NC*H*), 121.8 (NC*H*), 117.8 (*p*-C of pym.), 34.2 (N-CH_3). Anal. Calcd. for $C_8H_9N_4PF_6$: C, 31.37; H, 2.91; N, 18.30. Found: C, 31.32; H, 2.90; N, 18.28%.

*Synthesis of chloro (p-cymene)-1-methyl-3-pyrimidylimidazolideneruthenium(II)-hexaflurophosphate (**3a**):*

Preparation of **3a** was done following the transmetallation protocol[16a,16b,24e,34], similarly to our recent report[34]. Proligand **3** (0.15 g, 0.49 mmol) and black Ag_2O powder (0.06 g, 0.26 mmol) was stirred in 15~20 ml ACN for 5 h at room temperature, under exclusion of light. The resultant blend was then filtered with a G-4 filter to obtain a clear Ag-carbene complex solution and eliminate the untreated reagents. [Ru(*p*-cymene)Cl_2]$_2$ (0.15 g, 0.25 mmol) was dissolved in a minimum amount of ACN in round bottom flux and heated up to 120°C, and this solution freshly prepared solution of Ag-carbene complex was added dropwise, and the mixture was stirred in the same condition for 4 h. The yellowish-orange product indicates the formation of complex **3a**. The solution was then filtered to eliminate the AgCl. The yellowish-orange colored filtrate was evaporated to dryness to get the product to reduce of **3a**. The compound **3a** was recrystallized from ACN/diethyl ether. The orange, yellowish microcrystalline product was separated by filtration and washed several times with petroleum benzene. Yield was 87% (0.25 g, 0.43 mmol). ^{1}H NMR (DMSO-d_6, 25°C, 300 Mz): δ 9.72 (d, *J* 7.0 Hz, 2H, H$^{\alpha\text{-pym}}$), 8.73 (d, *J* 7.2 Hz, 1H, H^{imi}), 8.62 (d, *J* 7.1 Hz, 1H, H^{imi}), 7.85 (t, *J* 7.3 Hz, 1H, H$^{\beta\text{-pym}}$), 6.48(d, *J* 6.6 Hz, 4H, CH_{arom}), 3.12 (s, 3H, N-CH_3), 2.61 (m, 1H, CH_{arom}), 2.12 (s, 3H, -$CH_{3\ arom}$), 0.87–0.80 (m, 6H, -CH_3). ^{13}C NMR (DMSO-d_6, 100.5 MHz, 25°C, ppm) δ: 172.6 (*m*-C of pym.), 162.5 (NCH), 161.3 (*m*-C of pym.), 158.8 (C_{arbene}), 157.2 (*i*-C of pym.), 154.6 (*i*-C of pym.), 127.3 (NCH), 122.4 (NCH), 119.6 (*p*-C of pym.), 92.4, 90.3, 88.4, 84.5, 36.9 (N-CH_3), 22.6, 20.3, 19.3. Anal. Calcd. for $C_{18}H_{22}N_4RuClPF_6$, C, 37.52; H, 3.82; N, 9.72. Found: 37.22; H, 3.67; N, 9.57%.

Theoretical studies:

To get insightinto the electronic configuration and nature of absorption spectra of the complex **3a**, we have performed DFT computation using B3LYP/def2-TZVP level of the theory in the Gaussian 09W[62] suit. The imaginary frequency of the molecule comes out to zero, infer to corresponding energy minima structure on the potential energy surface[63]. The FMOs of the molecule were generated with Gauss view 6.0. During TD-DFT analysis upon UV-Vis spectra, pseudo potential on the metal (Ru) was included. PDOS was also calculated to scrutinize the structure-bonding relationship and the orbital contribution of Ru(II) and ligands towards the formation of FMOs.

*X-Ray structure determination of complex **3a**:*

Single-crystal X-ray diffraction data of complex **3a** was recorded, and diminution of data was performed using the Bruker SAINT program[64]. The data set was integrated with the Denzo-SMN package[65] and corrected for Lorentz, polarization, and absorption effects (SORTAV)[66]. The structure of **3a** was determined by direct methods (SIR97)[67] and refined using full-matrix least-squares with all non-hydrogen atoms anisotropically, and hydrogens were included in calculated positions riding on their carrier atoms. All calculations were carried out using SHELXL-97[68], PARST[69], and WINGX[70] programs. The CIF data was recorded at The Cambridge Crystallographic Data Centre with CCDC no. 824311 and available at http://www.ccdc.cam.ac.uk.

Cell viability assay:

For the *in vitro* cytotoxic evaluation of the Ru-NHC complex **3a**, human cancer cell lines (A549, MCF7, HCT116) and non-carcinoma embryonic fibroblast cells from healthy mice (3T3) were cultured and maintained at 37°C and 5% CO_2. Before treatment with the complex **3a**, cells (3000 cells per well) were plated in 96-well culture plates for 24 h. The cell lines were then treated with DMSO solution of complex **3a** at

increasing (0–100 μM) concentrations for 48 h. At the same time, the cells were also treated with 0.5% (v/v) DMSO and considered a control. After incubation, the MTT assay was used for cell viability analysis[34]. MTT reagent (20 μL of 5 mM MTT solution) was added in each and further incubated for 4 h at 37°C. The IC_{50} data were calculated from the plot of cell viability vs concentration of complex **3a**.

DNA cleavage study:

To explore the DNA-cleaving performance of molecule **3a**, its explicitaction to relax the plasmid DNA was investigated. The pTZ57R/T plasmid DNA was incubated with different complex **3a** concentrations. The study of DNA cleavage by the ruthenium compound **3a** over time was carried out to determine whether the direct double-strand cleaves further, and it is analyzed by Agarose gel Electrophoresis under the UV-Transilluminator.

Circular dichroism spectra:

CD spectra were recorded at 37°C using a Jasco J-810 CD spectropolarimeter, with the scanning rate 100 nm min^{-1}, and with response time 1 s. The scanning range was 350–190 nm, and the spectra were measured at standard sensitivity (100 mdeg) with a data pitch of 0.5 nm in unremitting mode. The other instrumental setup is followed as per our previous report[24e]. CD spectra were collected from the reaction mixture containing CT-DNA and Ru-compound **3a** in phosphate buffer (pH 7.2) incubated at 37°C for 12 h, and blank CT-DNA was used as control. All the spectral data recorded were the average of three consequent results.

Molecular docking simulations:

Molecular docking simulations were performed to predict the binding affinities and atomic interactions for the complex **3a** in contact with DNA and BCL-2. For this, the single crystal XRD structure of **3a** was optimized using Mercury v.3.8[71] software package, and the ruthenium atom, which is not supported in AutoDock 4.0 tools[72], was replaced by carbon atoms on Maestro v.10.2.011 (Schrodinger). Crystal structures of a DNA dodecamer (PDB entry: 1bna) and BCL-2 (PDB entry: 4lvt) were set as receptors using of (40×40×60) $Å^3$ and (40×40×40) $Å^3$ grid boxes, respectively[34]. Fifty runs of molecular docking simulations were programmed, and the complexes were ranked according to their binding affinities in kcal mol^{-1}. The highest affinity values for complex **3a**, BCL-2, and DNA were selected, and the respective ligand coordinate file (**3a** resulting from docking) was used as input in Maestro v.10.2.011 for ruthenium atom reintegration. The topologies for the final Ru(II)-complex **3a** were generated using PRODRG followed by energy minimization using the GROMOS96 43a2 force field from the GROMACS v.5.0.4 software package. The visualization of the molecular complexes and atomic interactions measurement were done using PyMOL v.2.0 software.

Conclusion

In summary, Ru(II)-NHC complex **3a**; [chloro(*p*-cymene)-1-methyl-3-pyrimidylimidazolideneruthenium(II)-hexafluorophosphate], was synthesized and structurally and functionally characterized. Complex **3a** shows excellent absorption spectra obeying mixed-mode metal-ligand transitions. It shows the irreversible oxidation character of the redox process in the cyclic voltammograms. This study also presents a new Ru(II)-NHC complex as to lead drug candidate against lung (A549), colon (HCT116), and breast (MCF7) cancer cell lines with optimistic cell viability results. All these findings were also supported by *in silico* studies. Therefore, we are confident that the data reported here can be used for further anticancer evaluations using Ru(II)-NHC complexes as an alternative to conventional treatments.

Abbreviation

ACN = Acetonitrile, THF = tetrahydrofuran, DMF = dimethylformamide, DMSO = dimethylsulfoxide, TMS = tetramethylsilane, en = ethylenediamine, DFT = density functional theory, TDDFT = time dependent DFT, PDOS = partial density of states, FMO = frontier molecular orbital, TBAH = tetrabutylammonium hexafluorophosphate, CD = circular dichroism, CTDNA = calf thymus DNA, MTT = 3-(4,5-dimethylthiazol-2-yl)-2,5-diphenyltetrazolium bromide, IC_{50} = half maximal inhibitory concentration.

Acknowledgments

B. Rana, wants to thank Haldia Institute of Technology (HIT), Haldia, for Laboratory infrastructure support during his PhD research work, and J. Dinda is grateful to the SERB, India, for financial support (SR/FT/CS-046/2009). The XRD data were collected at Indian Association for the Cultivation of Science, Kolkata, India. The authors would like to extend their heartfelt thanks to Dr. Santi M. Mandal, Central Research Facility, Indian Institute of Technology Kharagpur, India, for his guidance and help during biological analysis. The authors also acknowledge Fundação de Apoio à Pesquisa

do Distrito Federal (FAPDF), Coordenação de Aperfeiçoamento de Pessoal de Nível Superior (CAPES), Conselho Nacional de Desenvolvimento e Tecnológico (CNPq) and Fundação de Apoio ao Desenvolvimento do Ensino, Ciência e Tecnologia do Estado de Mato Grosso do Sul (FUNDECT), Brazil.

The scheme was designedby B. Rana, G. Roymahapatra, and J. Dinda. All the compounds were synthesized and characterized by B. Rana. Absorption spectra and cyclovotametry analyses were carried out by B. Rana, H. S. Das and P. K. Mahapatra. G. Roymahapatra and S. Giri did the theoretical analysis and DFT study. B. Rana did biological analysis with the guidance of Dr. Santi M. Mandal, IIT Kharagpur. M. H. Cardoso and O. L. Franco carried out computational simulations. P. P. Bag carried out crystal data analysis.

References

1. (a) B. Rosenberg, L. Vancamp, J. E. Trosko and V. H. Mansour, *Nature,* 1969, **222**, 385; (b) G. Jaouen and A. Vessieres, *Pure Appl. Chem.*, 1985, **57**, 1865.
2. J. Reedijk, *Chem. Rev.,* 1999, **99**, 2499.
3. (a) Y. W. Jung and S. J. Lippard, *Chem. Rev.*, 2007, **107**, 1387; (b) D. Wang and S. J. Lippard, *Nat. Rev. J. Drug Discovery*, 2005, **4**, 307; (c) J. Reedijk, *Platinum Met. Rev.*, 2008, **52**, 2; (d) J. Reedijk, *Curr. Opin. Chem. Biol.,* 1999, **3**, 236; (e) J. Reedijk, *Proc. Natl. Acad. Sci. USA,* 2003, **100**, 3611.
4. (a) M. Auzias, B. Therrien, G. S. Fink, P. Sÿtě pnič ka, W. H. Ang and P. J. Dyson, *Inorg. Chem.*, 2008, **47**, 578 and ref. therein; (b) S. P. Fricker, *Dalton Trans.,* 2007, 4903.
5. B. Lippert, "*Cis*platin, Chemistry and Biochemistry of a Leading Anticancer Drug", Wiley-VCH, Weinheim, 1999.
6. (a) A. Levina, A. Mitra and P. A. Lay, *Metallomics*, 2009, **1**, 458; (b) G. S. Fink, *Dalton Trans.,* 2010, **39**, 1673; (c) J. Will, A. kyas, W. S. Sheldrick and D. Wolters, *J. Bio. Inorg. Chem.,* 2007, **12**, 883; (d) A. Casini, G. Mastrobuoni and M. Terenghi, *J. Bio. Inorg. Chem.*, 2007, **12**, 1107; (e) A. Casini, A. Guerri, C. Gabbiiani and L. Messori, *J. Inorg. Biochem.*, 2002, **108**, 995.
7. M. J. Clarke, *Met. Ions Biol. Syst.,* 1980, **11**, 231.
8. M. J. Clarke, F. Zhu and D. R. Frasca, *Chem. Rev.,* 1999, **99**, 2511.
9. A. D. Kelman, M. J. Clarke, S. D. Edmonds and H. J. Persie, *J. Clin. Hematol. Oncol.,* 1977, **7**, 274.
10. C. S. Allardyce and P. J. Dyson, *Platinum Metals Rev.*, 2001, **45**, 62.
11. A. J. Arduengo III, R. L. Harlow and M. Kline, *J. Am. Chem. Soc.*, 1991, **113**, 361.
12. (a) M. N. Hopkinson, C. Richter, M. Schedler and F. Glorius, *Nature*, 2014, **510**, 485; (b) M. Fèvre, J. Pinaud, Y. Gnanou, J. Vignolle and D. Taton, *Chem. Soc. Rev.*, 2013, **42**, 2142; (c) E. Peris, *Chem. Rev.*, 2018, **118**, 9988.
13. (a) J. Izquierdo, G. E. Hutson, D. T. Cohen and K. A. Scheidt, *Angew. Chem., Int. Ed.*, 2012, **51(47)**, 11686; (b) D. T. Cohen and K. A. Scheidt, *Chem. Sci.*, 2011, **3(1)**, 53; (c) H. D. Velazquez and F. Verpoort, *Chem. Soc. Rev.*, 2012, **41(21)**, 7032.
14. (a) L. Oehninger, R. Rubbiani and I. Ott, *Dalton Trans.*, 2013, **42(10)**, 3269; (b) W. Liu and R. Gust, *Chem. Soc. Rev.*, 2013, **42(2)**, 755; (c) A. Gautier and F. Cisnetti, *Metallomics*, 2012, **4(1)**, 23; (d) J. C. Y. Lin, R. T. W. Huang, C. S. Lee, A. Bhattacharyya, W. S. Hwang and I. J. B. Lin*, Chem. Rev.*, 2009, **109(8)**, 3561.
15. L. Mercs and M. Albrecht, *Chem. Soc. Rev.*, 2010, **39(6)**, 1903.
16. (a) G. Roymahapatra, S. M. Mandal, W. F. Porto, T. Samanta, S. Giri, J. Dinda, O. L. Franco and P. K. Chattaraj, *Curr. Med. Chem.*, 2012, **19(24)**, 4184; (b) T. Samanta, G. Roymahapatra, W. F. Porto, S. Seth, S. Ghorai, S. Saha, J. Sengupta, O. L. Franco, J. Dinda and S. M. Mandal, *PLOS One*, 2013, **8**, e58346; (c) C. R. Shahini, G. Achar, S. Budagumpi, M. Tacke and S. A. Patil, *Appl. Organomet. Chem.*, 2017, **31**, e3819.
17. (a) B. Rosenberg, L. Vancamp, J. E. Trosko and V. H. Mansour, *Nature*, 1969, **222**, 385; (b) M.-L. Teyssot, A.-S. Jarrousse, M. Manin, A. Chevry, S. Roche, F. Norre, C. Beaudoin, L. Morel, D. Boyer, R. Mahiou and A. Gautier, *Dalton Trans*, 2009, 6894.
18. (a) C. V. Maftei, E. Fodor, P. G. Jones, M. Freytag, M. H. Franz, G. Kelter, H. H. Fiebig, M. Tamm and I. Neda, *Euro. J. Med. Chem.*, 2015, **101**, 431; (b) F. Hackenberg and M. Tacke, *Dalton Trans.*, 2014, **43**, 8144; (c) K. M. Hindi, T. J. Siciliano, S. Durmus, M. J. Panzner, D. A. Medvetz, D. V. Reddy, L. A. Hogue, C. E. Hovis, J. K. Hilliard, R. Mallett, C. A. Tessier, C. L. Cannon and W. J. Youngs, *J. Med. Chem.*, 2008, **51**, 1577; (d) Ö. Karaca, V. Scalcon, S. M. Meier Menches, R. Bonsignore, J. M. J. L. Brouwer, F. Tonolo, A. Folda, M. P. Rigobello, F. E. Kühn and A. Casini, *Inorg. Chem.*, 2017, **56**, 14237.
19. (a) J. C. Garrison and W. J. Youngs, *Chem. Rev.*, 2005, **105**, 3978; (b) A. K. Nebioglu, M. J. Panzner, C. A. Tessier, C. L. Cannon and W. J. Youngs, *Coord. Chem. Rev.*, 2007, **251**, 884.
20. (a) F. Cisnetti and A. Gautier, *Chem. Int. Ed.*, 2013, **52**, 11976; (b) A. Muhammad, M. M. Mehboob, A. A. A. Seliman, A. A. Isab, V. Dhuna, G. Bhatia and K. Dhuna, *J. Organomet. Chem.*, 2014, **765**, 68.
21. (a) C. K. Mirabelli, R. K. Johnson, D. T. Hill, L. F. Faucette, G. R. Girard, G. Y. Kuo, C. M. Sung and S. T. Crooke, *J. Med. Chem.*, 1986, **29**, 218; (b) T. M. Simon, D. H. Kunishima, G. J. Vibert and A. Lorber, *Cancer*, 1979, **44**, 1965; (c) M. Porchia, M. Pillai, M. Marinelli, F. Tisato, F. D. Bello and C. Santini, *Euro. J. Med. Chem.*, 2018, **146**, 709.

22. (a) N. H. Kim, H. J. Park, M. K. Oh and I. S. Kim, *BMB Rep*., 2013, **46**, 59; (b) J. R. Roberts, J. Xiao, B. Schliesman, D. J. Parsons and C. F. Shaw, *Inorg. Chem*., 1996, **35**, 424.
23. (a) E. Schuh, C. Pflüger, A. Citta, A. Folda, M. PiaRigobello, A. Bindoli, A. Casini and F. Mohr, *J. Med. Chem.*, 2012, **55**, 5518; (b) P. J. Barnard and S. J. Berners-Price, *Coord. Chem. Rev.*, 2007, **251**, 1889; (c) S. Ray, R. Mohan, J. K. Singh, M. K. Samantaray, M. Shaikh, D. Panda and P. Ghosh, *J. Am. Chem. Soc.*, 2007, **129**, 15042; (d) T. V. Serebryanskaya, A. S. Lyakhov, L. S. Ivashkevich, J. Schur, C. Frias, A. Prokop and I. Ott, *Dalton Trans*., 2015, **44**, 1161; (e) J. L. Hickey, R. A. Ruhayel, P. J. Barnerd, M. V. Baker, S. J. Berners-Price and A. Filipovska, *J. Am. Chem. Soc.*, 2008, **130**, 12570; (f) B. Bertrand, L. Stefan, M. Pirrotta, D. Monchaud, E. Bodio, P. Richard, P. L. Gendre, E. Warmerdam, M. H. de Jager, G. M. M. Groothuis, M. Picquet and A. Casini, *Inorg. Chem*., 2014, **53**, 2296.
24. (a) A. Levina, A. Mitra and P. A. Lay, *Metallomics*, 2008, **1**, 458; (b) G. S. Fink, *Dalton Trans*., 2010, **39**, 1673; (c) J. Will, A. Kyas, W. S. Sheldrick and D. Wolters, *J. Bio. Inorg. Chem*., 2007, **12**, 883; (d) A. Casini, G. Mastrobuoni and M. Terenghi, *J. Bio. Inorg. Chem*., 2007, **12**, 1107; (e) G. Roymahapatra, J. Dinda, A. Mishra, A. Mahapatra, W.-S. Hwang and S. M. Mandal, *J. Cancer Res. Ther.*, 2015, **11**, 105; (f) A. Casini, A. Guerri, C. Gabbiiani and L. Messori, *J. Inorg. Biochem*., 2002, **108**, 995.
25. M. J. Clarke, *Met. Ions Biol. Syst.*, 1980, **11**, 231.
26. M. J. Clarke, F. Zhu and D. R. Frasca, *Chem. Rev*., 1999, **99**, 2511.
27. (a) R. Vilaplana, M. Romero, M. Quiros, J. Salas and F. Gonzalez-Vilches, *Metal-Based Drugs,* 1995, **2**, 211; (b) D. Chatterjee, A. Mitra and G. S. De, *Platinum Met. Rev*., 2006, **50**, 2; (c) E. Alessio, G. Mestroni, G. Nardin, W. M. Attia, M. Calligaris, G. Sava and S. Zorzet, *Inorg. Chem.*, 1988, **27**, 4099; (d) G. Sava, S. Pacor, S. Zorzet, E. Alessio and G. Mestroni, *Pharmacol. Res*., 1989, **21(5)**, 617; (e) M. Coluccia, G. Sava, F. Loseto, A. Nassi, A. Bocarelli, D. Giordano, E. Alessio and G. Mestroni, *Eur. J. Cancer*, 1993, **29**, 1873; (f) A. H. Velders, H. Kooijman, A. L. Spek, J. G. Haasnoot, D. de Vos and J. Reedijk, *Inorg. Chem.,* 2000, **39**, 2966; (g) A. C. G. Hotze, E. P. L. van der Geer, S. E. Caspers, H. Kooijman, A. L. Spek, J. G. Haasnoot and J. Reedijk, *Inorg. Chem*., 2004, **43(16)**, 4935.
28. E. Reisner, V. B. Arion, B. K. Keppler and A. J. L. Pombeiro, *Inorg. Chim. Acta*, 2008, **361**, 1569.
29. A. D. Kelman, M. J. Clarke, S. D. Edmonds and H. J. Persie, *J. Clin. Hematol. Oncol*., 1977, **7**, 274.
30. (a) S. P. Fricker, *Dalton Trans*., 2007, 4903; (b) M. J. Clarke and H. Taube, *J. Am. Chem. Soc*., 1974, **96**, 5413.
31. Y. Hung, W. J. Kung and H. Taube, *Inorg. Chem.,* 1981, **20**, 457.
32. F. Wang, J. Bella, J. Parkinson and P. J. Sadler, *J. Biol. Inorg. Chem*., 2005, **10**, 147.
33. (a) H. Chen, A. J. Parkinson, R. E. Morris and P. J. Sadler, *J. Am. Chem. Soc*., 2003, **125**, 173; (b) S. A. Patil, A. P. Hoagland, S. A. Patil and A. Bugarin, *Future Medicinal Chemistry,* 2020, **12(24)**. https://doi.org/10.4155/fmc-2020-0175.
34. B. K. Rana, G. Roymahapatra, H. S. Das, S. Giri, M. H. Cardoso, O. L. Franco, N. K. Kiran, M. K. Santra, P. P. Bag, V. Bertolasi and J. Dinda, *J. Mol Structure*, 2021, **1231**, 129822. https://doi.org/10.1016/j.molstruc.2020.129822.
35. T. Samanta, B. K. Rana, G. Roymahapatra, S. Giri, P. Mitra, R. Pallepogu, P. K. Chattaraj and J. Dinda, *Inorg. Chim. Acta,* 2011, **375**, 271.
36. D. Gnanamgari, E. L. O. Sauer, N. D. Schley, C. Butler, C. D. Incarvito and R. H. Crabtree, *Organometallics*, 2009, **28**, 321.
37. T. A. Khan, K. Bhar, R. Thirumoorthi, T. K. Roy and A. K. Sharma, *New J. Chem*., 2020, **44**, 239.
38. D. Meyer, M. A. Taige, A. Zeller, K. Hohlfeld, S. Ahrens and T. Strassner, *Organometallics,* 2009, **28**, 2142.
39. J. Ye, W. Chen and D. Wang, *Dalton Trans*., 2008, 4015.
40. M. Poyatos, E. M. Marzá, M. Sanaú and E. Peris, *Inorg. Chem.,* 2004, **43**, 1793.
41. F. Saleem, G. K. Rao, S. Kumar, M. P. Singh and A. K. Singh, *Dalton Trans*., 2015, **44**, 19141.
42. D. Gnanamgari, E. L. O. Sauer, N. D. Schley, C. Butler, C. D. Incarvito and R. H. Crabtree, *Organometallics,* 2009, **28**, 321.
43. (a) S. D. Adhikary, T. Samanta, G. Roymahapatra, F. Loiseau, D. Jouvenot, S. Giri, P. K. Chattaraj and J. Dinda, *New J. Chem.*, 2010, **34**, 1974; (b) G. Roymahapatra, D. Sarkar, A. Nandi, S. Giri, T. K. Mondal, A. Mahapatra, W.-S. Hwang and J. Dinda, *J. Indian Chem. Soc*., 2012, **92(1)**, 79.
44. (a) R. Parida, S. Das, L. J. Karas, J. I-C. Wu, G. Roymahapatra and S. Giri, *Inorg. Chem. Front*., 2019, **6**, 3336; (b) K. Kajiwara, S. Yamane, T. Haraguchi, S. Pradhan, C. Sinha, R. Parida, S. Giri, G. Roymahaptra, D. Moon and T. Akitsu, *J. Chem. Chem. Eng*., 2019, **13**, 23; (c) R. Parida, G. N. Reddy, A. Ganguly, G. Roymahapatra, A. Chakraborty and S. Giri, *Chem. Commun*., 2018, **54**, 3903.
45. S. D. Adhikary, D. Bose, P. Mitra, K. D. Saha, V. Bertolasi and J. Dinda, *New J. Chem*., 2012, **36**, 759.
46. W. H. Ang, E. Baldini, L. J. Jeanneret and P. J. Dyson, *Inorg. Chem*., 2007, **46**, 9048.
47. S. M. Mandal, L. Migliolo, S. Das, M. Mandal, O. L. Franco and T. K. Hazra, *J. Cell Biochem.*, 2012, **113**, 184.
48. L. Ronconi and P. J. Sadler, *Coord. Chem. Rev*., 2007, **251**, 1633.
49. S. Dhar and S. J. Lippard, *PNAS*, 2009, **106**, 22199.

50. C. Gao, S. Gou and G. Xu, *Chem. Pharm. Bull*., 2011, **59**, 851.

51. X. G. Sun, E. H. Cao, X. Y. Zhang, D. D. Liu and C. Bai, *Inorg. Chem. Commun.,* 2002, **5**, 181.

52. (a) P. J. Dyson, *Chimia*., 2007, **61**, 698; (b) S. J. Dougan and P. J. Sadler, *Chimia.*, 2007, **61**, 704; (c) L. D. Dale, J. H. Tocher, T. M. Dyson, D. I. Edwards and D. A. Tocher, *Anticancer Drug Des.*, 1992, **7**, 3.

53. (a) W. H. Ang and P. J. Dyson, *Eur. J. Inorg. Chem*., 2006, **20**, 4003; (b) L. Zeng, P. Gupta, Y. Chen, E. Wang, L. Ji, H. Chao and Z.-S. Chen, *Chem. Soc. Rev*., 2017, **46**, 5771.

54. R. K. Gupta, A. Kumar, R. P. Paitandi, R. S. Singh, S. Mukhopadhyay, S. P. Verma, P. Das and D. S. Pendley, *Dalton Trans*., 2016, **45**, 7163.

55. N. R. Palepu, S. L. Nongbri, J. R. Premkumar, A. K. Verma, K. Bhattacharjee, S. R. Joshi, S. Forbes, Y. Mozharivskyj, R. Thounaojam, K. Aguan and M. R. Kollipara, *J. Biol. Inorg. Chem.*, 2015, **20**, 619.

56. (a) K. Lin, Z.-Z. Zhao, H-B. Bo, X.-J. Hao and -Q. Wang, *Front Pharmacol*., 2018, **9**, 1323. doi: 10.3389/fphar.2018.01323; (b) M. Pongratz, P. Schluga, M. A. Jakupec, V. A. Arion, C. G. Hartinger, G. Allmaier and B. K. Keppler, *J. Anal. At. Spectrom*., 2004, **37**, 46.

57. (a) L. Messori, F. G. Vilchez, R.Vilaplana, F. Piccioli, E. Alessio and B. K. Keppler, *Metal-Based Drugs*, 2000, **7**, 335; (b) A. R. Timerbaev, C. G. Hartinger, S. S. Aleksenko and B. K. Keppler, *Chem. Rev*., 2006, **106**, 2224; (c) P. Schluga, C. G. Hartinger, A. Egger, E. Reisner, M. Galanski, M. A. Jakupec and B. K. Keppler, *Dalton Trans*., 2006, **14**, 1796.

58. (a) K. Kajiwara, S. Pradhan, T. Haraguchi, C. Sinha, R. Parida, S. Giri, G. Roymahaptra and T. Akitsu, *Symmetry*, 2020, **12(5)**, 797. doi: 10.3390/sym12050797; (b) G. Roymahapatra, National Seminar - 'New Horizon in Biotechnology -2019', 2019, ISBN 978-81-927768-3-5, 101; (c) T. Chowdhury, G. Roymahapatra and S. M. Mandal, *Infectious Disorders - Drug Targets*, doi: 10.2174/1871526520666200727153643.

59. A. J. Souers, J. D. Leverson, E. R. Bogaert, S. L. Ackler, N. D. Catron, J. Chen, B. D. Dayton, H. Ding, S. H. Enschede, W. J. Fairbrother, D. C. Huang, S. G. Hymowitz, S. Jin, S. L. Khaw, P. J. Kovar, L. T. Lam, J. Lee, H. L. Maecker, K. C. Marsh, K. D. Mason, M. J. Mitten, P. M. Nimmer, A. Oleksijew, C. H. Park, C. M. Park, D. C. Phillips, A. W. R. Roberts, D. Sampath, J. F. Seymour, M. L. Smith, G. M. Sullivan, S. K. Tahir, C. Tse, M. D. Wendt, Y. Xiao, J. C. Xue, H. Zhang, R. A. Humerickhouse, S. H. Rosenberg and S. W. Elmore, *Nat. Med*., 2013, **19**, 202.

60. H. R. Drew, R. M. Wing, T. Takano, C. Broka, S. Tanaka, K. Itakura and R. E. Dickerson, *Proc. Natl. Acad. Sci. USA*, 1981, **78**, 2179.

61. Y. B. Ouyang and R. G. Giffard, *Neurochem. Int*., 2014, **77**, 2.

62. Gaussian 09, Revision D.01, Gaussian, Inc., Wallingford CT, 2013.

63. (a) M. Tripathi, G. C. Giri, D. Das, R. Pande, S. Sarkar, S. Giri, G. Roymahapatra and A. Sarkar, *Nucleosides Nucleotides Nucleic Acids*, 2018, **37(10)**, 563; (b) A. Ghosh, G. Roymahapatra, D. Paul and S. M. Mandal, *Comput. Biol. Chem.*, 2020, **87**, 107275(1-9). doi: 10.1016/j.compbiolchem.2020.107275; (c) T. Chowdhury, J. Dutta, S. M. Mandal and G. Roymahapatra, *J. Indian Chem. Soc*., 2020, **97**, 1279.

64. Bruker (2002) SAINT (Version 6.36a) Bruker AXS Inc. Madison, Wisconsin, USA.

65. (a) Z. Otwinowski and W. Minor, *Methods in Enzymology*, 1997, **276**, 307; (b) S. J. Williams, V. Notenboom, J. Wicki, D. R. Rose and S. G. Withers, *J. Am. Chem. Soc*., 2000, **122(17)**, 4229.

66. (a) R. H. Blessing, *Acta Cryst.,* 1995, A**51**, 33. doi: 10.1107/S0108767394005726; (b) A. Altomare, M. C. Burla, M. Camalli, G. L. Cascarano, C. Giacovazzo, A. Guagliardi, A. G. G. Moliterni, G. Polidori and R. J. Spagna, *Appl. Cryst.*, 1999, **32**, 115.

67. M. Nardelli, *J. Appl. Crystallogr*, 1995, **28**, 659.

68. G. M. Sheldrick, SHELX-97, University of Gottingen, Germany, 1997.

69. A. L. Spek, *Acta Cryst.,* 2009, **D65**, 148.

70. L. J. Farrugia, *J. Appl. Crystallogr.*, 1999, **32**, 837.

71. C. F. Macrae, P. R. Edgington, P. McCabe, E. Pidcock, G. P. Shields, R. Taylor, M. Towler and J. van de Streek, *J. Appl. Cryst*., 2006, **39**, 453.

72. O. Trott and A. J. Olson, *J. Comput. Chem*., 2010, **31**, 455.